Bone Marrow Metastases: T2-weighted Dixon Spin-Echo Fat Images Can Replace T1-weighted Spin-Echo Images[1]

Yaël Maeder, MD
Vincent Dunet, MD
Raphael Richard, MD
Fabio Becce, MD
Patrick Omoumi, MD, MSc, PhD

Purpose: To test the potential of Dixon T2-weighted fat-only sequences to replace T1-weighted sequences for the detection of bone metastases, with the hypothesis that diagnostic performance with an alternative magnetic resonance (MR) imaging protocol (sagittal spin-echo Dixon T2-weighted fat-only and water-only imaging) would not be inferior to that with the standard protocol (sagittal spin-echo T1-weighted and spin-echo Dixon T2-weighted water-only imaging).

Materials and Methods: A total of 121 consecutive whole-spine MR imaging examinations (63 men; mean age ± standard deviation, 61.4 years ± 11.8) performed for suspected vertebral bone metastases were included in this retrospective, institutional review board–approved study. Quantitative image analysis was performed for 30 randomly selected spine levels. Qualitative analysis was performed separately by two musculoskeletal radiologists, who registered the number of metastases for each spine level. Areas under the curve with the protocols were compared on the basis of nonparametric receiver operating characteristic curve estimations by using a noninferiority test on paired data, with a best valuable comparator as a reference. Interobserver and interprotocol agreement was assessed by using κ statistics.

Results: Contrast-to-noise ratio was significantly higher on the alternative protocol images than on the standard protocol images (181.1 [95% confidence interval: 140.4, 221.7] vs 84.7 [95% confidence interval: 66.3, 103.1] respectively; $P < .001$). Diagnostic performance was not significantly inferior with the alternative protocol than with the standard protocol for both readers in a per-patient analysis (sensitivity, 97.9%–98.9% vs 93.6%–97.9%; specificity, 85.2%–92.6% vs 92.6%–96.3%; area under the curve, 0.92–0.96 vs 0.95, respectively; all $P \leq .02$) and a per–spine level analysis (all $P < .01$). Interobserver and interprotocol agreement was good to very good (κ = 0.70–0.81).

Conclusion: Dixon T2-weighted fat-only and water-only imaging provide, in one sequence, diagnostic performance similar to that of the standard combination of morphologic sequences for the detection of probable spinal bone metastases, thereby providing an opportunity to reduce imaging time by eliminating the need to perform T1 sequences.

An earlier incorrect version of this article appeared online. This article was corrected on November 6, 2017.

[1] From the Department of Diagnostic and Interventional Radiology, Lausanne University Hospital, Rue du Bugnon 46, 1011 Lausanne, Switzerland. Received February 9, 2017; revision requested April 7; revision received June 30; accepted July 11; final version accepted August 16. **Address correspondence to** P.O. (e-mail: *Patrick.omoumi@chuv.ch*).

Magnetic resonance (MR) imaging is considered a technique of reference for the evaluation of bone marrow involvement for a large variety of solid tumors (1–3). Although acquisition protocols greatly vary among institutions, there is a common consensus that the standard protocol for the detection and characterization of bone metastases should include a combination of T1-weighted and fat-suppressed fluid-sensitive sequences (1–10). The T1-weighted sequences are aimed at assessing the replacement of the normal fatty components of the bone marrow with the neoplastic cellular proliferation, whereas fat-suppressed fluid-sensitive sequences increase the sensitivity for lesion detection (2,4,8).

Different types of fat-suppression techniques exist, including chemical shift–selective fat saturation, or CHESS; short inversion time inversion-recovery, or STIR; and the Dixon technique (11). The Dixon, or chemical shift–based water-fat separation, technique exploits the chemical shift between protons of water and fat to decompose the signal from these two tissues in the same voxel, generating a set of four images: in-phase (equivalent to standard non–fat-suppressed images), out-of-phase, water-only, and fat-only (equivalent to fat-suppressed) images (12–14). The Dixon technique was first described in 1984, and recent developments have allowed different variations of this technique to emerge as valid fat-suppression methods in clinical routine spin-echo (SE) imaging (12). In musculoskeletal applications, Dixon SE imaging has been mostly used to provide more homogeneous fat suppression than is achieved with CHESS, notably with large fields of view, such as in spine imaging, and higher signal-to-noise ratio than with STIR imaging (11,15–21). In addition, Dixon SE T2-weighted water-only images have shown low sensitivity to susceptibility artifacts and performance similar to that of T2-weighted CHESS and STIR techniques in detecting pathologic spinal abnormalities (16,19,22). As a consequence, Dixon T2-weighted water-only imaging of the spine is increasingly used to provide fat-suppressed, fluid-sensitive contrast.

An additional advantage of Dixon techniques is the ability to provide, in one acquisition, several series of images with different contrasts (ie, both non–fat-suppressed and fat-suppressed images). This approach has been used in various musculoskeletal applications to decrease imaging times (15,16,19,23). On the basis of the rationale that fat-only images generated with the Dixon technique could provide the same information on bone marrow replacement lesions as can T1-weighted sequences, we hypothesized that the standard protocol for the detection of bone marrow metastases could be reduced to a single Dixon T2-weighted sequence, thereby providing an opportunity to reduce acquisition time. To test the potential of Dixon fat-only images to replace T1-weighted images for the detection of spinal metastases, we hypothesized that the diagnostic performance with an alternative MR imaging protocol (sagittal SE Dixon T2-weighted fat-only and water-only imaging) would not be inferior to that with the standard protocol (sagittal SE T1-weighted and SE Dixon T2-weighted water-only images).

Advance in Knowledge

- For both readers, the Dixon T2-weighted fat-only and water-only imaging was not inferior to T1-weighted and Dixon T2-weighted water-only imaging for the detection of probable spinal bone marrow metastases in a per-patient analysis (sensitivity, 97.9%–98.9% vs 93.6%–97.9%; specificity, 85.2%–92.6% vs 92.6%–96.3%; area under the curve, 0.92–0.96 vs 0.95; all $P \leq .02$).

Implications for Patient Care

- Dixon spin-echo T2-weighted sequences with fat-only and water-only reconstructions can replace the standard combination of morphologic sequences (T1-weighted and fat-suppressed fluid sensitive) for the detection of probable spinal bone marrow lesions.
- Use of a Dixon spin-echo T2-weighted sequence as the only morphologic sequence for the detection of spinal bone metastases represents an opportunity to reduce imaging time.

Materials and Methods

Patient Population

Our single-center study was approved by our institutional ethics committee (Swiss Ethics Committees on research involving humans, Project ID 2016–00934), which did not require informed consent because of the retrospective design. We retrospectively included all adult patients who underwent whole-spine MR imaging for the assessment of spinal metastases in our institution from September 2014 to April 2016. Figure 1 describes patient flow and characteristics. We excluded all examinations from patients with a history of hematologic neoplasia or spinal osteosynthesis, examinations with incomplete MR imaging protocols, and those performed with 1.5-T MR imagers. Most of our spine MR imaging examinations are performed with 3-T

https://doi.org/10.1148/radiol.2017170325

Content codes: MK MR

Radiology 2018; 286:948–959

Abbreviations:
AUC = area under the curve
CI = confidence interval
SE = spin echo

Author contributions:
Guarantor of integrity of entire study, P.O.; study concepts/study design or data acquisition or data analysis/interpretation, all authors; manuscript drafting or manuscript revision for important intellectual content, all authors; approval of final version of submitted manuscript, all authors; agrees to ensure any questions related to the work are appropriately resolved, all authors; literature research, Y.M., R.R., F.B., P.O.; clinical studies, Y.M., V.D., R.R., P.O.; statistical analysis, Y.M., V.D., P.O.; and manuscript editing, Y.M., V.D., F.B., P.O.

Conflicts of interest are listed at the end of this article.

Figure 1

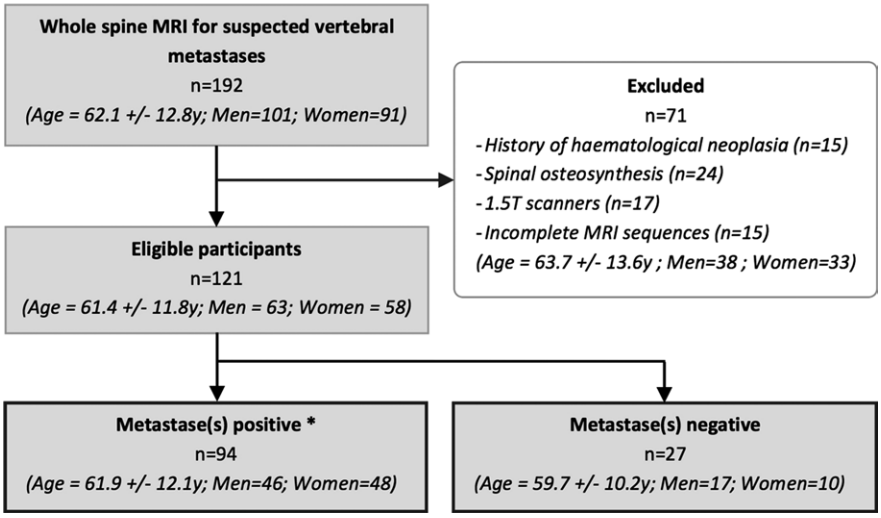

Figure 1: Flowchart shows selection and characteristics of patients. * = primary tumors included non–small cell lung ($n = 22$), breast ($n = 20$), melanoma ($n = 10$), prostate ($n = 8$), pancreas ($n = 6$), epidermoid ($n = 5$), liver ($n = 5$), parotid ($n = 5$), colorectal ($n = 4$), esophagogastric ($n = 5$) small-cell lung ($n = 4$), kidney ($n = 3$), thyroid ($n = 3$), bladder ($n = 2$), germ cell ($n = 2$), and soft-tissue sarcoma ($n = 1$).

Table 1

MR Imaging Acquisition Parameters

Parameter	Fast SE T1-weighted Imaging	Fast SE T2-weighted Dixon
Plane	Sagittal	Sagittal
No. of sections	19–23	19–23
Section thickness (mm)	3	3
Gap (mm)	0.3–0.6	0.3–0.6
Field of view (mm)	260 × 260–285 × 285	260 × 260–285 × 285
Acquisition matrix	384 × 384–448 × 448	320 × 320–320 × 350
Phase-encoding direction	Head to feet	Head to feet
Repetition time/echo time (msec)	555–668/10–11	4340–4820/88–92
Turbo factor	4	17–18
No. of averages	1	1–2
IPAT factor	2	2–3
Phase oversampling	0.8	0.6–1
Flip angle (degrees)	147–160	137–150
Bandwidth (Hz/pixel)	210–217	340–372
Acquisition time (min:sec)	4:20 ± 0:22	9:25 ± 1:24

Note.—Numeric data are range values obtained from a random selection of 30 examinations. IPAT = integrated parallel acquisition technique.

imagers, and we aimed at maintaining homogeneity of our sample.

MR Imaging Examinations

All MR imaging examinations were performed with commercially available imagers operating at 3 T (Verio, Skyra, Prisma; Siemens, Erlangen, Germany) without hardware modifications and with the imagers' radiofrequency body coils. Imaging parameters of the sequences of interest are detailed in Table 1. A total of three contiguous sagittal stacks with nonenhanced fast SE T1-weighted and fast SE Dixon T2-weighted sequences of the entire spine from the base of the skull to the last sacral piece were performed for all patients. Four sets of images were routinely reconstructed from the Dixon T2 sequences: in-phase, out-of-phase, Dixon T2-weighted water-only, and Dixon T2-weighted fat-only images, of which only the latter two were considered for our study. Additional sequences performed on a case-by-case basis whenever indicated were considered only for the best valuable comparator. They included contrast material–enhanced fat-suppressed T1-weighted sequences on the sagittal and axial planes, as well as axial fat-suppressed T2-weighted sequences.

Quantitative Image Analysis

To quantitatively compare image quality and the conspicuity of bone metastases on T1-weighted and Dixon T2-weighted fat-only images, 30 spine levels (from 30 different patients) with focal metastases (according to the best valuable comparator as described below) were randomly selected. On each level, the largest lesion was used to calculate signal-to-noise and contrast-to-noise ratios on T1-weighted and Dixon T2-weighted fat-only images by a final-year radiology resident (Y.M., with 5 years of experience). A 30-mm^2 region of interest was placed on the area of metastasis and the closest area of normal bone marrow that could fit the region of interest. A third region of interest of 30 mm^2 was placed within ghost-free regions of background outside the patient, as close as possible to the metastasis. Signal-to-noise and contrast-to-noise ratios were computed according to the following formulas: $SNR = SI_{bone\ marrow}/N$, $CNR = (SI_{metastasis} - SI_{bone\ marrow})/N$, where SNR is signal-to-noise ratio, CNR is contrast-to-noise ratio, $SI_{bone\ marrow}$ and $SI_{metastasis}$ are the mean signal intensity inside the region of interest placed on normal bone marrow and the area of metastasis, respectively, and N is the noise, defined as the standard deviation of the background signal intensity outside the patient.

Qualitative Image Analysis

Image analysis was performed by two fellowship-trained musculoskeletal radiologists (P.O. and R.R., with 8 and 3 years of experience, respectively) who were blinded to the clinical data. The two protocols were assessed separately and independently by the two radiologists during two different reading sessions that were held 1 month apart with imaging examinations in a random order. Each cervical, thoracic, lumbar, and sacral level was assessed separately for the number of metastatic lesions regardless of their size. The cervical and lumbar levels were defined as the seven first and five last mobile vertebral segments, whether there were or were not any transitional vertebrae. The number of metastases was recorded, from zero to five or more, with segments with more than five metastases considered as one group of five or more metastases. Complete involvement of all spinal segments (referred to as diffuse bone marrow involvement) was encoded separately. Metastasis was defined as an area of replacement of the fatty signal of bone marrow, hypointense compared with skeletal muscle on T1-weighted images, and without detectable signal intensity on Dixon T2-weighted fat-only images (Figs 2–5) (2). As described in the literature, the fat-suppressed T2-weighted images (Dixon T2-weighted water-only images) were read in correlation with the previous "fat-sensitive" sequences to improve sensitivity by detecting foci of increased signal intensity and to help characterize indeterminate lesions (2).

Figure 2

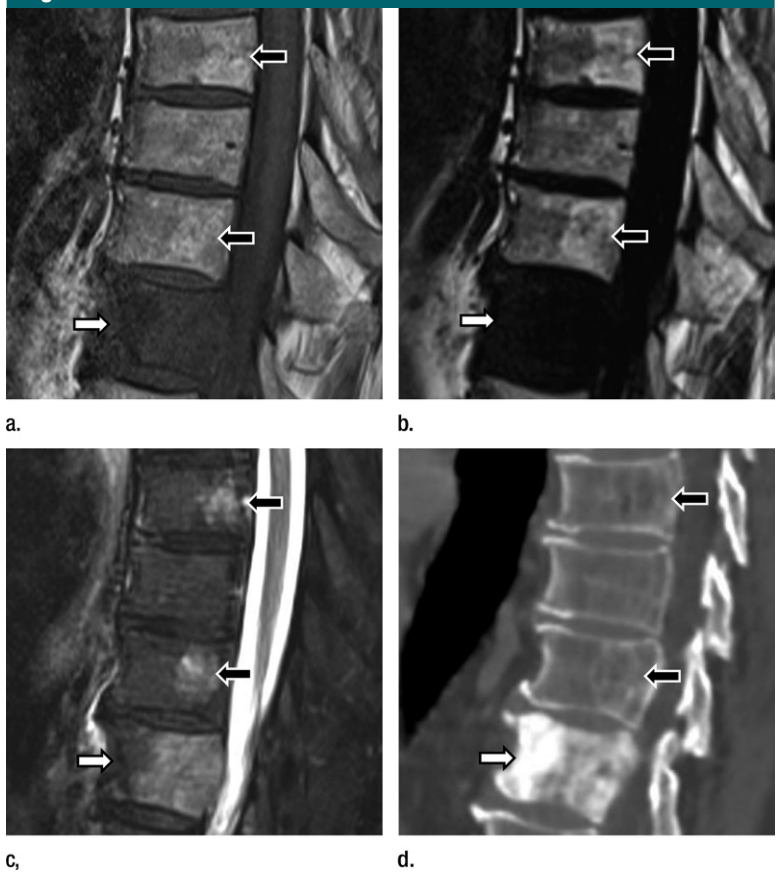

Figure 2: Images in an 81-year-old man with prostate cancer and sclerotic bone metastases. Sagittal thoracic spine MR images include **(a)** T1-weighted, **(b)** Dixon T2-weighted fat-only, and **(c)** Dixon T2-weighted water-only sequences. **(d)** Unenhanced computed tomographic (CT) image obtained the day after MR imaging, with sagittal reformat, is also shown. Sclerotic metastasis on thoracic spine (white arrow) shows signal intensity slightly hypointense to adjacent paravertebral muscles on **a**, and no detectable intralesional signal intensity is visible on **b**. Better conspicuity of lesion on **b** is supported by higher contrast-to-noise ratio at quantitative analysis (56 for **a** vs 118 for **b**). Note two vertebral hemangiomas (black arrows), unchanged over 2 years compared with previous CT images (not shown), with typical thickened trabeculae at CT (black arrows in **d**), appearing slightly hyperintense relative to normal marrow on **a** and clearly hyperintense on **b** image.

Best Valuable Comparator

The reference standard for the presence or absence of metastases was based on a best valuable comparator (24–27). The best valuable comparator consisted of the consensus reading of all examinations by the two musculoskeletal radiologists (performed 1 month after the end of all readings), as well as the review of all available medical data. These data included clinical, histologic (spinal bone biopsy data, available for 30 patients), biologic, and imaging data. The mean follow-up time was 15.2 months after the MR imaging examination (minimum follow-up time, 8.0 months). In the rest of this report, we will refer to the areas likely to be metastases according to this reference standard simply as metastases.

False-Negative and False-Positive Results

To analyze causes of false-positive and false-negative results with each protocol, the two readers retrospectively analyzed all cases of false-positive and false-negative findings on a per-patient basis in order to determine the causes of interpretation errors (more than one cause possible per patient).

Statistical Analysis

Before inclusion of patients, sample size was calculated. On the basis of previous studies, we assumed an area under the curve (AUC) of 0.95 for the standard MR imaging protocol and considered that a difference as large as 0.1 in favor of the standard MR imaging protocol would still allow the alternative MR imaging protocol to be noninferior (24). We calculated

Figure 3

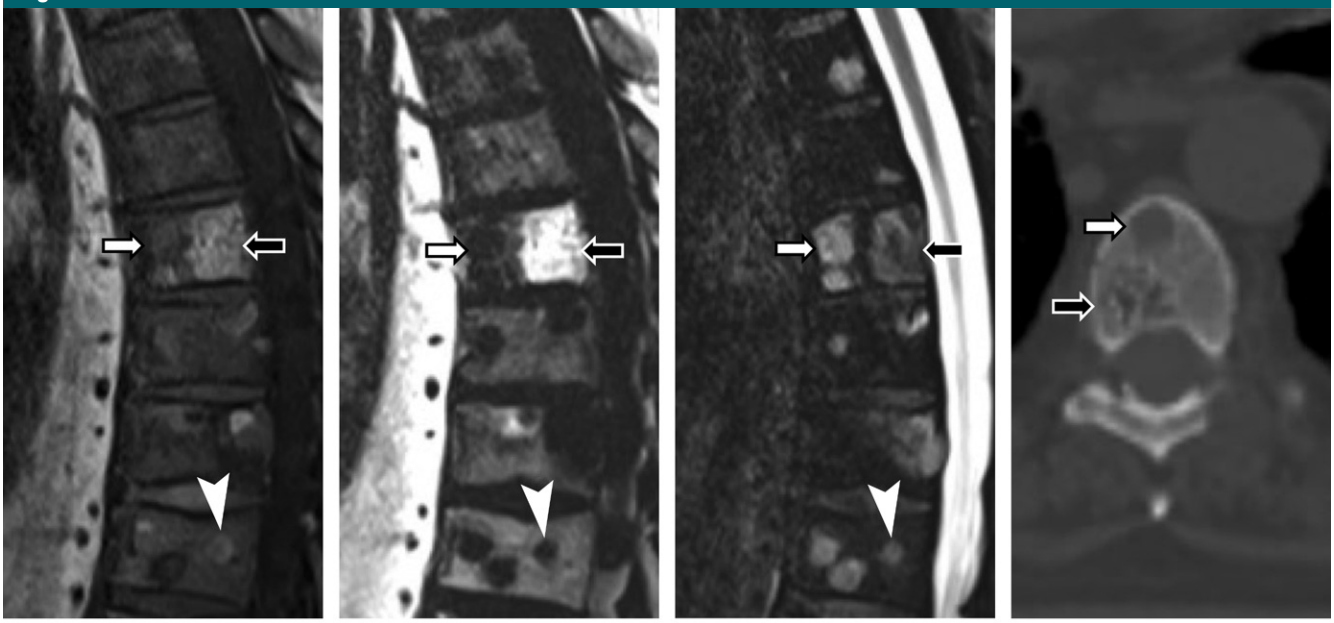

a. b. c. d.

Figure 3: Images in a 66-year-old man with malignant melanoma and lytic bone metastases. Sagittal thoracic spine MR images including **(a)** T1-weighted, **(b)** Dixon T2-weighted fat-only, and **(c)** Dixon T2-weighted water-only sequences. **(d)** Unenhanced CT image obtained within 3 months of MR imaging, with axial reformat, is also shown. Multiple spinal metastases are visible, all showing high signal intensity on **c** (white arrow and arrowhead) and with no detectable intralesional signal intensity on **b** (white arrow and arrowhead), whereas signal intensity varies on **a**, with some lesions appearing isointense or hyperintense relative to skeletal muscle (arrowhead). Note that on **b**, hemangioma (black arrow) cannot be differentiated by its signal intensity from metastases on **c**, whereas it shows fatty content on **a** and **b**. **(d)** CT image shows lytic metastasis (white arrow) and confirms presence of hemangioma (black arrow), with typical thickened trabeculae, which was unchanged over 1 year when compared with previous CT images (not shown).

a sample size of 76 patients to achieve a power of 80% to confirm noninferiority by using a one-sided *z*-test at a significance level of .05. For the quantitative image analysis, signal-to-noise and contrast-to-noise ratios from the standard and alternative protocols were compared with the Wilcoxon signed-rank test. For the qualitative image analysis, diagnostic performance values (sensitivity, specificity, AUC, positive likelihood ratio, negative likelihood ratio, positive and negative predictive values) and respective 95% confidence intervals (CIs) were determined for each reader and each protocol in comparison with the best valuable comparator as our standard of reference, on a per-patient basis and per–spine level basis. For each reader, AUCs with the standard and alternative protocols were compared on the basis of estimation of a nonparametric receiver operating characteristic curve by using a noninferiority test on paired data (H_0: $AUC_{alt} - AUC_{stan} \leq -0.1$; H_1: $AUC_{alt} - AUC_{stan} > -0.1$, where AUC_{alt} and AUC_{stan} are the AUCs of the alternative and standard protocols; noninferiority margin: 0.1) (28). The differences between AUCs of the alternative and standard protocols were calculated, along with 95% CIs of the differences. Interobserver agreement for each protocol and interprotocol agreement for each reader for the number of metastatic lesions were assessed by using the weighted Cohen κ coefficient, interpreted by using the Landis and Koch scale (<0 indicated no agreement; 0–0.20, slight agreement; 0.21–0.40, fair agreement; 0.41–0.60, moderate agreement; 0.61–0.80, good agreement; and ≥0.81, very good agreement) (29). Diagnostic performance and interobserver and interprotocol agreement were estimated for each spine level (cervical, thoracic, lumbar, and sacral) to detect any regional influence. A *P* value of less than .05 was considered to indicate a statistically significant difference for all tests. To test for a difference in age between men and women, a Kruskal-Wallis test for equality was performed. All statistical tests were performed with software (Stata 13.1; Stata, College Station, Tex).

Results

Best Valuable Comparator

We included 121 patients (mean age ± standard deviation, 61.4 years ± 11.8; 63 men [mean age, 62.8 years ± 12.2], 58 women [mean age, 59.9 years ± 11.1]; no statistical difference in age between men and women [$P = .25$]) suspected of having spinal bone metastases (Fig 1). Eighty patients were examined for spinal symptoms in a known oncologic context, and 41 patients were examined for systematic screening. Among these 121 patients, 94 received

Figure 4

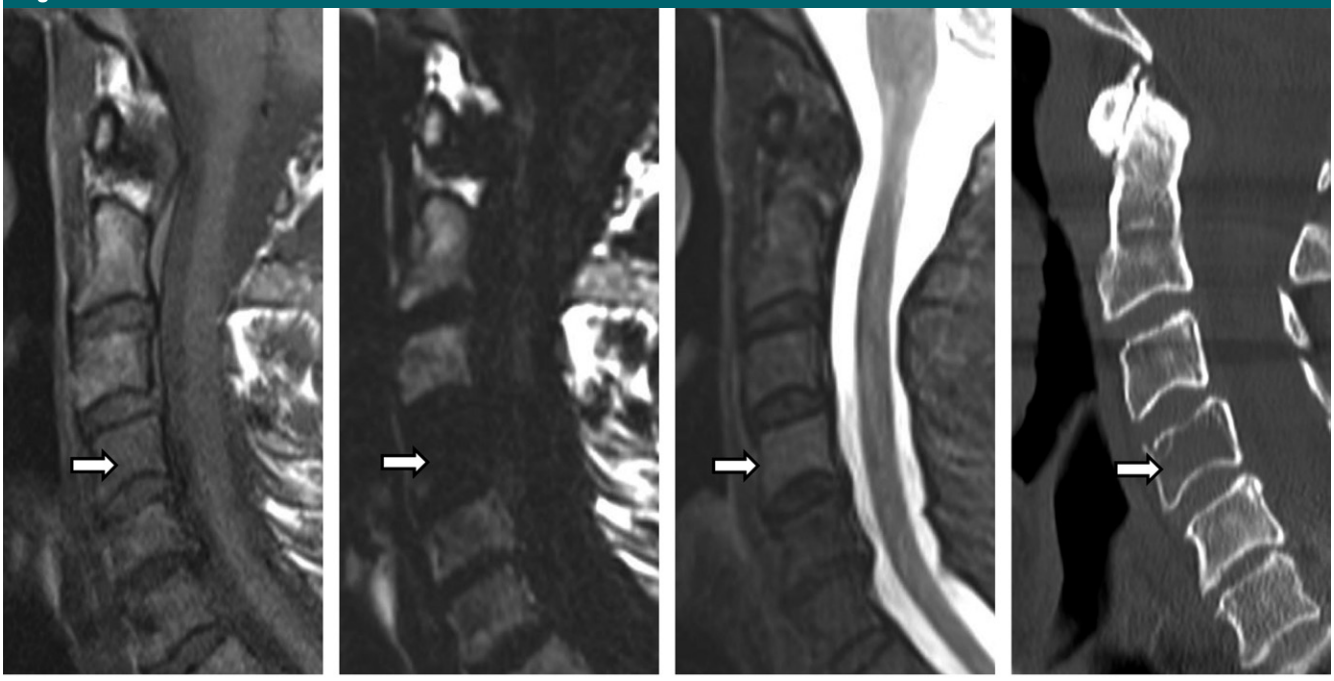

a. b. c. d.

Figure 4: Images in a 64-year-old man with multifocal hepatocellular carcinoma. Sagittal cervical spine MR images include **(a)** T1-weighted, **(b)** Dixon T2-weighted fat-only, and **(c)** Dixon T2-weighted water-only images. **(d)** Unenhanced CT image obtained 4 months after MR imaging, with sagittal reformat, is also shown. Lytic metastasis (arrow), confirmed on **d**, is clearly visible on **b,** with focal absence of signal intensity, whereas it was missed by both readers with standard protocol. Better conspicuity of lesion on **b** was supported by higher contrast-to-noise ratio (22 for **a** vs 108 for **b**) at quantitative analysis.

a positive diagnosis for metastates according to the best valuable comparator (Fig 1), including 43, 81, 77, and 55 with metastases in the cervical, thoracic, lumbar spine, and sacrum, respectively. Overall, there were a total of at least 725 metastases, because we considered as one group the segments with at least five metastases (the exact number was not known). There were at least 102, 254, 234, and 135 metastases in the cervical, thoracic, and lumbar spine, and sacrum, respectively. Nine patients had diffuse metastatic involvement of the spinal bone marrow.

Quantitative Analysis

The mean signal intensity from metastases was 259.0 (95% CI: 226.2, 291.7) for T1-weighted images and 16.1 (95% CI: 11.4, 20.1) for Dixon T2-weighted fat-only images. The mean signal intensity from normal bone marrow was 515.8 (95% CI: 454.1, 611.2) and 305.2 (95% CI: 252.4, 358.0), respectively. Signal-to-noise ratios did not differ significantly between the T1-weighted and Dixon T2-weighted fat-only images (174.3 [95% CI: 149.8, 198.8] vs 191.9 [95% CI: 149.5, 234.4], respectively; P = .19), whereas the contrast-to-noise ratio was significantly higher for the Dixon T2-weighted fat-only images vs T1-weighted images (181.1 [95% CI: 140.4, 221.7] vs 84.7 [95% CI: 66.3, 103.1] respectively; $P < .001$) (Figs 2 and 4).

Qualitative Analysis

Per-patient analysis.—On a per-patient basis (Table 2), the diagnostic performance for classifying a patient as having metastasis was not significantly inferior for the alternative protocol compared with the standard protocol ($P < .001$ for reader 1 and $P \leq .02$ for reader 2).

Per–spine level analysis.—Detailed diagnostic performance parameters for the two protocols are reported in Table 3. For all spine levels, the alternative protocol was not significantly inferior to the standard protocol (all P values < 0.01).

Interprotocol Agreement

The agreement for both readers between protocols was good for all spine levels (κ values ranged from 0.70 [95% CI: 0.65, 0.81] to 0.79 [95% CI: 0.68, 0.82]) (Table 4).

Interobserver Agreement

The agreement between readers for both protocols was good or very good for all spine levels (κ values ranged from 0.71 [95% CI: 0.61, 0.76] to 0.81 [95% CI: 0.75, 0.87]) (Table 4).

False-Negative and False-Positive Results

A total of 11 and five patients had false-negative and false-positive findings, respectively. Eight cases of false-negative results with the standard protocol included 28 lesions with posttreatment intralesional fatty content (mistaken for hemangiomas or focal red marrow

Figure 5

a. b. c. d.

Figure 5: Images in a 55-year-old woman with breast cancer and diffuse mixed lytic and sclerotic bone metastases. Sagittal thoracic spine MR images include **(a)** T1-weighted, **(b)** Dixon T2-weighted fat-only, and **(c)** Dixon T2-weighted water-only images. **(d)** Positron emission tomographic)/CT image obtained within 1 month of MR imaging, with sagittal reformat, is also shown. Diffuse involvement of thoracic spine, confirmed on **d**, is visible on **a** as diffuse decrease of signal intensity, lower than adjacent muscles and is clearly shown on **b** as absence of any signal intensity on vertebral bodies. Note absence of significant pathologic signal intensity on **c**.

hyperplasia) and six lesions adjacent to disks (mistaken for Schmorl nodules). Three cases of false-negative results with the alternative protocol included eight lesions previously treated and two lesions adjacent to disks. Cases of false-positive results with the standard protocol (n = 1) and the alternative protocol (n = 4) included lesions adjacent to disks (n = 2 and 10, respectively).

Discussion

The results of this study showed the potential of Dixon T2-weighted fat-only imaging to replace T1-weighted sequences for the detection of spinal bone marrow metastases by revealing that diagnostic performance with images reconstructed from the Dixon sequence (Dixon T2-weighted fat-only and water-only) was not inferior to the performance of the standard protocol (T1-weighted and Dixon T2-weighted water-only). This represents an opportunity to reduce imaging time, which would be highly beneficial for the comfort of patients suspected of having spinal bone metastases. Of note, the diagnostic performance of both protocols in our study was similar to or superior to previously reported performance of MR imaging for the detection of bone marrow metastases (reported sensitivity and specificity, 77%–100% and 88–100%, respectively) (3,24,25,30–32).

Fat is a fundamental component of bone marrow, present in both yellow and red marrow (which contains approximately 40% fat cells and 60% hematopoietic cells) (5). The cellular proliferation in metastatic lesions locally replaces normal bone marrow, leading to the disappearance of fatty MR imaging signal inside the lesion; this has been established as a key diagnostic criterion to differentiate neoplastic tissue from normal marrow (2,33). The importance of the contribution of fat to bone marrow signal explains the importance of nonenhanced T1-weighted sequences (on which fat shows high signal intensity) for the evaluation of bone marrow: Hypointense metastatic lesions are well demarcated from the background of high–signal intensity normal fatty marrow (2,3,7,34). Although the signal intensity of malignant lesions (the so-called bone marrow replacement lesions) can vary widely on fluid-sensitive sequence images, it is usually decreased on T1-weighted images. This decrease in signal intensity should be interpreted relative to the signal of skeletal muscle to differentiate neoplastic lesions from red bone marrow with different degrees of cellularity (34).

Because Dixon T2-weighted fat-only images are specific to fat signal, their interpretation is more straightforward: Bone marrow replacement lesions show almost no intralesional signal relative to adjacent bone marrow because of the disappearance of fat, and there is no need to compare the signal intensity to that of adjacent muscle. Interestingly, the detection of melanoma metastases is also straightforward on Dixon T2-weighted fat-only images, with consistent loss of signal intensity, whereas it represents a classic pitfall on T1-weighted images because of the shortening of T1 according to melanin content. These considerations on the interpretation of signal intensity on T1-weighted and Dixon T2-weighted fat-only images were supported by the

Table 2

Diagnostic Performance with Standard and Alternative Protocols for Each Reader: Per-Patient Analysis

Reader, Protocol	Sensitivity (%)	Specificity (%)	AUC	LR+	LR−	PPV (%)	NPV (%)	Difference between AUCs*	PValue†
Reader 1									
Standard	97.9 (92.5, 99.7) [92/94]	92.6 (75.7, 99.1) [25/27]	0.95 (0.90, 1.0)	13.2 (3.5, 50.2)	0.02 (0.01, 0.09)	97.9 (92.5, 99.7) [92/94]	92.6 (75.7, 99.1) [25/27]		
Alternative	98.9 (94.2, 100) [93/94]	92.6 (75.7, 99.1) [25/27]	0.96 (0.91, 1.0)	13.4 (3.5, 50.7)	0.01 (0.002, 0.08)	97.9 (92.6, 99.7) 93/95]	96.2 (80.4, 99.9) [25/26]	0.01 (−0.01, 0.02)	<.001
Reader 2									
Standard	93.6 (86.6, 97.6) [88/94]	96.3 (81.0, 99.9) [26/27]	0.95 (0.91, 0.99)	25.3 (3.7, 173)	0.07 (0.03, 0.1)	98.9 (93.9, 1.0) [88/89]	81.3 (63.6, 92.8) [26/32]		
Alternative	97.9 (92.5, 99.7) [92/94]	85.2 (66.3, 95.8) [23/27]	0.92 (0.85, 0.99)	6.6 (2.7, 16.3)	0.03 (0.01, 0.1)	95.8 (89.7, 98.9) [92/96]	92.0 (74.0, 99.0) [23/25]	−0.03 (−0.10, 0.03)	.022

Note.—Data are diagnostic performance parameters, with 95% CIs in parentheses. Wherever applicable, raw values are reported in brackets. The best valuable comparator was taken as the reference standard. LR+ = positive likelihood ratios [sensitivity/(1 − specificity)]; LR− = negative likelihood ratios [(1 − sensitivity)/specificity]; NPV = negative predictive value; PPV = positive predictive value.

* Between those with standard and alternative protocols.

† *P* values refer to noninferiority test on paired data for nonparametric receiver-operating characteristic curve estimations.

quantitative analysis, showing intralesional signal intensity close to zero on Dixon T2-weighted fat-only images, and significantly higher contrast-to-noise ratios for lesions on the Dixon T2-weighted fat-only images compared with that on T1-weighted images. Of note, most false-negative and false-positive findings were due to previously treated metastases. Indeed, previous chemotherapy or radiation therapy might induce the appearance of intralesional fat, which could lead to false-negative results (35). This pitfall must be kept in mind when bone marrow imaging results are being reported.

Recently, results of other studies have demonstrated the increased lesion conspicuity on Dixon T2-weighted fat-only images in musculoskeletal applications. Results of one study (15) showed higher contrast-to-noise ratio of Dixon T2-weighted fat-only images compared with that on T1-weighted images for the detection of periarticular fat deposition in patients with chronic sacroiliitis. In another study (17), authors compared lesion conspicuity on Dixon T1-weighted fat-only images and T1-weighted images in a small number of metastases (n = 38), with qualitative and quantitative lesion conspicuity significantly higher on Dixon T1weighted fat-only images than on T1-weighted images ($P < .01$). However, to the best of our knowledge, our study is the first to specifically assess the ability of bone marrow fat imaging provided by the Dixon T2-weighted fat-only images to replace conventional T1-weighted sequences.

Other advantages of using T2-weighted Dixon sequences, previously described in the literature, are worth mentioning. Indeed, Dixon T2-weighted sequences provide two additional series (in-phase and out-of-phase reconstructions) that can be useful in the characterization of bone lesions and the complications of metastases, such as vertebral compression fractures, at no additional cost in terms of imaging time. First, the in-phase Dixon T2-weighted reconstructions are equivalent to non–fat-suppressed T2-weighted images, providing anatomic information that compensates for the relative lack of conspicuity of vertebral or spinal canal anatomy on Dixon T2-weighted fat-only

Table 3

Diagnostic Performance with Standard and Alternative Protocols for Each Reader: Per–Spine Level Analysis

Spine Level, Reader, Protocol	Sensitivity (%)	Specificity (%)	AUC	LR+	LR−	PPV (%)	NPV (%)	Difference between AUCs*	*P* Value†
Cervical									
Reader 1									
Standard	81.4 (66.6, 91.6) [35/43]	89.7 (80.8, 95.5) [70/78]	0.86 (0.79, 0.92)	7.9 (4.1, 15.5)	0.2 (0.1, 0.4)	81.4 (66.6, 91.6) [35/43]	89.7 (80.8, 95.5) [70/78]		
Alternative	88.4 (74.9, 96.1) [38/43]	93.6 (85.7, 97.9) [73/78]	0.91 (0.85, 0.97)	13.8 (5.9, 32.4)	0.1 (0.05, 0.3)	88.4 (74.9, 96.1) [38/43]	93.6 (85.7, 97.9) [73/78]	0.05 (−0.01, 0.10)	<.001
Reader 2									
Standard	83.7 (69.3, 93.2) [36/43]	89.7 (80.8, 95.5) [70/78]	0.87 (0.80, 0.93)	8.2 (4.2, 15.9)	0.2 (0.09, 0.4)	81.8 (67.3, 91.8) [36/44]	90.9 (82.2, 96.3) [70/77]		
Alternative	90.7 (77.9, 97.4) [39/43]	92.3 (84.0, 97.1) [72/78]	0.92 (0.86, 0.97)	11.8 (5.4, 25.6)	0.1 (0.04, 0.3)	86.7 (73.2, 94.9) [39/45]	94.7 (87.1, 98.5) [72/76]	0.05 (−0.00, 0.1)	<.001
Thoracic									
Reader 1									
Standard	95.1 (87.8, 98.6) [77/81]	92.5 (79.6, 98.4) [37/40]	0.94 (0.89, 0.99)	12.7 (4.3, 37.7)	0.05 (0.02, 0.1)	96.3 (89.4, 99.2) [77/80]	90.2 (76.9, 97.3) [37/41]		
Alternative	93.8 (86.2, 98.0) [76/81]	92.5 (79.6, 98.4) [37/40]	0.93 (0.88, 0.98)	12.5 (4.2, 37.2)	0.07 (0.03, 0.2)	96.2 (89.3, 99.2) [76/79]	88.1 (74.4, 96.0) [37/42]	−0.01 (−0.05, 0.04)	<.001
Reader 2									
Standard	91.4 (83.0, 96.5) [74/81]	95.0 (83.1, 99.4) [38/40]	0.93 (0.89, 0.98)	18.3 (4.7, 70.7)	0.09 (0.04, 0.2)	97.4 (90.8, 99.7) [74/76]	84.4 (70.5, 93.5) [38/45]		
Alternative	95.1 (87.8, 98.6) [77/81]	90.0 (76.3, 97.2) [36/40]	0.93 (0.87, 0.98)	9.5 (3.8, 24.1)	0.05 (0.02, 0.1)	95.1 (87.8, 98.6) [77/81]	90 (76.3, 97.2) [36/40]	−0.01 (−0.05, 0.03)	<.001
Lumbar									
Reader 1									
Standard	94.8 (87.2, 98.6) [73/77]	95.5 (84.5, 99.4) [42/44]	0.95 (0.91, 0.99)	20.9 (5.4, 80.9)	0.05 (0.02, 0.1)	97.3 (90.7, 99.7) [73/75]	91.3 (79.2, 97.6) [42/46]		
Alternative	97.4 (90.9, 99.7) [75/77]	93.2 (81.3, 98.6) [41/44]	0.95 (0.91, 1.0)	14.3 (4.8, 42.6)	0.03 (0.01, 0.1)	96.2 (89.2, 99.2) [75/78]	95.3 (84.2, 99.4) [41/43]	0.00 (−0.04, 0.04)	<.001
Reader 2									
Standard	90.9 (82.2, 96.3) [70/77]	95.5 (84.5, 99.4) [42/44]	0.93 (0.89, 0.98)	20.0 (5.2, 77.6)	0.1 (0.05, 0.2)	97.2 (90.3, 99.7) [70/72]	85.7 (72.8, 94.1) [42/49]		
Alternative	96.1 (89, 99.2) [74/77]	90.9 (78.3, 97.5) [40/44]	0.94 (0.89, 0.98)	10.6 (4.2, 26.9)	0.04 (0.01, 0.1)	94.9 (87.4, 98.6) [74/78]	93.0 (80.9, 98.5) [40/43]	0.00 (−0.05, 0.06)	<.001

Table 3 *(continues)*

Table 3 (continued)

Spine Level, Reader, Protocol	Sensitivity (%)	Specificity (%)	AUC	LR+	LR−	PPV (%)	NPV (%)	Difference between AUCs*	*P* Value†
Sacral									
Reader 1									
Standard	92.7 (82.4, 98.0) [51/55]	97.0 (89.5, 99.6) (64/66)	0.95 (0.91, 0.99)	30.6 (7.8, 120)	0.08 (0.03, 0.2)	96.2 (87.0, 99.5) [51/53]	94.1 (85.6, 98.4) [64/68]		
Alternative	90.9 (80.0, 97.0) [50/55]	93.9 (85.2, 98.3) [62/66]	0.92 (0.88, 0.97)	15.0 (5.8, 38.9)	0.1 (0.04, 0.2)	92.6 (82.1, 97.9) [50/54]	92.5 (83.4, 97.5) [62/67]	−0.02 (−0.08, 0.03)	.004
Reader 2									
Standard	90.9 (80.0, 97.0) [50/55]	97.0 (89.5, 99.6) [64/66]	0.94 (0.90, 0.98)	30.0 (7.6, 118)	0.09 (0.04, 0.2)	96.2 (86.8, 99.5) [50/52]	92.8 (83.9, 97.6) [64/69]		
Alternative	85.5 (73.3, 93.5) [47/55]	97.0 (89.5, 99.6) [64/66]	0.92 (0.86, 0.96)	28.2 (7.2, 111)	0.15 (0.08, 0.3)	95.9 (86.0, 99.5) [47/49]	88.9 (79.3, 95.1) [64/72]	−0.03 (−0.08, 0.02)	.003

Note.—Data are diagnostic performance parameters, with 95% CIs in parentheses. Wherever applicable, raw values are reported in brackets. The best valuable comparator was taken as the reference standard. LR+ = positive likelihood ratios [sensitivity/(1 − specificity)]; LR− = negative likelihood ratios [(1 − sensitivity)/specificity]; NPV = negative predictive value; PPV = positive predictive value.

* Between those with standard and alternative protocols.

† *P* values refer to noninferiority test on paired data for nonparametric receiver-operating characteristic curve estimations.

images. This anatomic information is useful for the delineation of the vertebral body contours to detect pathologic fractures or any involvement of the spinal canal (16,19). Second, the analysis of bone marrow heterogeneity on in-phase images can help characterize hyperplastic red marrow (which typically manifests low signal intensity compared with the adjacent fatty marrow on SE T2-weighted sequences) (5). Third, the comparison of signal intensity between in-phase and out-of-phase images is helpful in characterizing the neoplastic nature of a focal lesion or of a pathologic vertebral compression fracture (6,18,36,37). Neoplastic lesions show a signal dropout on out-of-phase images due to the replacement of intravoxel microscopic fatty components of the bone marrow (18,38). In particular, chemical-shift MR imaging was recently shown to be highly sensitive (sensitivity, 91.7%) in classifying indeterminate spinal bone lesions as malignant (18). The evaluation of the added value of these ancillary series was beyond the scope of our study, but these may contribute to the usefulness of the Dixon technique in clinical practice.

The strengths of our study include the assessment of a large number of patients, with a variety of primary solid tumors, including treated and untreated lesions and lytic and sclerotic metastases, reflecting clinical practice. We backed our results with measurement of objective image quality. Furthermore, compared with previous studies in which assessment was limited to certain metastases only, we assessed each metastasis individually and compared the performance of two readers to a reference standard (17).

Our study also had several limitations. First, the retrospective nature resulted in a lack of standardization of MR imaging acquisition parameters, which led to heterogeneity of the imaging acquisition protocol. Second, although readers were blinded to the clinical data, and the readings of the two protocols were carried out independently from each other in a random order, readers could not be blinded to the type of the sequence being analyzed; this might have resulted in a bias. Third, although

Table 4

Interprotocol Agreement and Interobserver Agreement for Number of Lesions at Each Spine Level

	Interprotocol Agreement κ		Interobserver Agreement κ	
Spine Level	Reader 1	Reader 2	Protocol 1	Protocol 2
Cervical	0.79 (0.68, 0.82)	0.77 (0.74, 0.82)	0.76 (0.65, 0.84)	0.78 (0.71, 0.83)
Thoracic	0.75 (0.71, 0.86)	0.70 (0.65, 0.81)	0.71 (0.61, 0.76)	0.81 (0.74, 0.86)
Lumbar	0.77 (0.75, 0.82)	0.72 (0.69, 0.74)	0.76 (0.70, 0.84)	0.81 (0.75, 0.87)
Sacral	0.76 (0.72, 0.82)	0.76 (0.69, 0.80)	0.81 (0.79, 0.81)	0.78 (0.76, 0.82)

Note.—Data are Cohen κ coefficients, with 95% CIs in parentheses. Interprotocol agreement refers to agreement between protocols for each reader; interobserver agreement refers to agreement between readers for each protocol. The number of lesions were categorized on a scale of 1–6 (one to five or more focal lesions, with category six as diffuse bone marrow involvement).

the examinations in our study were performed with a variety of MR imagers, we only assessed the diagnostic performance of the Dixon T2 sequence for the detection of metastases at 3 T with imagers from one manufacturer. Different manufacturers have developed their own methods for Dixon imaging, which might affect image quality. Fourth, because of the impossibility of obtaining systematic histologic proof for every metastatic lesion, we used the best valuable comparator as our reference standard. This parameter is commonly used in the context of studies dealing with diagnostic accuracy in the oncologic setting (24–27). In case of a difference in sensitivity between the sequences, this type of reference standard could create a bias against the sequence with lowest sensitivity, which was not the case in our study. Fifth, we did not adjust for multiple comparisons. Sixth, we did not assess the intraobserver agreement for the two protocols. However, assessment of intraobserver agreement is usually not required when interobserver agreement is high, as we found in our study (39). Finally, we limited our evaluation to adult patients because of the higher prevalence of bone metastases in this population. As a result of age-related changes in spinal marrow, the values reported for adults might be different from those for children, although these changes probably affect the aspect of metastases for both T1-weighted and Dixon fat-only images equally (40).

In conclusion, our results support the potential for Dixon T2-weighted fat-only images reconstructed from the Dixon SE T2-weighted sequence obtained in the standard protocol to replace T1-weighted imaging for the detection of bone marrow metastases, thereby allowing shortened routine acquisition protocols. This adds to the previously described advantages of other series of imaging with this technique, suggesting that one SE Dixon T2-weighted sequence could be the only morphologic sequence required for the detection and characterization of bone marrow metastases. On the basis of these results, a screening protocol for spinal metastases could be limited to sagittal Dixon SE T2-weighted sequences of the whole spine. To improve sensitivity for the detection of bone marrow metastases, the addition of a Dixon SE T2-weighted sequence on the coronal plane covering the pelvis and proximal femurs is recommended (8,41). Additional sequences (acquisition on the axial plane, gadolinium-enhanced sequences) can be added on a case-by-case basis to assess any spinal canal involvement detected with this screening protocol. Finally, recent literature supports an increase in sensitivity of MR imaging in detecting spinal metastases with the addition of functional sequences, such as diffusion-weighted sequences, to the standard morphologic imaging protocol (9,10). However, data suggest that diffusion-weighted sequences cannot replace but can only complement the morphologic part of the protocol, which was the focus of our study (9,10,42).

Future research should be performed to assess whether the Dixon T2-weighted fat-only images can replace T1-weighted sequences in other applications, such as the evaluation of intralesional fat content of primary musculoskeletal tumors or in the context of whole-body MR imaging (33). Furthermore, in our experience, the replacement of T1-weighted sequences with Dixon T2-weighted fat-only imaging can be generalized to all MR imaging applications aimed at the detection of bone marrow replacement lesions, including those at 1.5 T. This must be proven scientifically in future studies.

Disclosures of Conflicts of Interest: Y.M. disclosed no relevant relationships. **V.D.** disclosed no relevant relationships. **R.R.** disclosed no relevant relationships. **F.B.** disclosed no relevant relationships. **P.O.** disclosed no relevant relationships.

References

1. Ghanem N, Uhl M, Brink I, et al. Diagnostic value of MRI in comparison to scintigraphy, PET, MS-CT and PET/CT for the detection of metastases of bone. Eur J Radiol 2005;55(1):41–55.
2. Howe BM, Johnson GB, Wenger DE. Current concepts in MRI of focal and diffuse malignancy of bone marrow. Semin Musculoskelet Radiol 2013;17(2):137–144.
3. Lecouvet FE. Whole-body MR imaging: musculoskeletal applications. Radiology 2016;279(2):345–365.
4. Mirowitz SA, Apicella P, Reinus WR, Hammerman AM. MR imaging of bone marrow lesions: relative conspicuousness on T1-weighted, fat-suppressed T2-weighted, and STIR images. AJR Am J Roentgenol 1994;162(1):215–221.
5. Vande Berg BC, Malghem J, Lecouvet FE, Maldague B. Magnetic resonance imaging of normal bone marrow. Eur Radiol 1998;8(8):1327–1334.
6. Shah LM, Hanrahan CJ. MRI of spinal bone marrow: part I, techniques and normal age-related appearances. AJR Am J Roentgenol 2011;197(6):1298–1308.
7. Hanrahan CJ, Shah LM. MRI of spinal bone marrow: part 2, T1-weighted imaging-based differential diagnosis. AJR Am J Roentgenol 2011;197(6):1309–1321.
8. Lecouvet FE, Larbi A, Pasoglou V, et al. MRI for response assessment in metastatic bone disease. Eur Radiol 2013;23(7):1986–1997.

9. Pasoglou V, Michoux N, Tombal B, Jamar F, Lecouvet FE. wbMRI to detect bone metastases: critical review on diagnostic accuracy and comparison to other imaging modalities. Clin Transl Imaging 2015;3(2):141–157.

10. Padhani AR, Lecouvet FE, Tunariu N, et al. METastasis reporting and data system for prostate cancer: practical guidelines for acquisition, interpretation, and reporting of whole-body magnetic resonance imaging-based evaluations of multiorgan involvement in advanced prostate cancer. Eur Urol 2017;71(1):81–92.

11. Del Grande F, Santini F, Herzka DA, et al. Fat-suppression techniques for 3-T MR imaging of the musculoskeletal system. RadioGraphics 2014;34(1):217–233.

12. Dixon WT. Simple proton spectroscopic imaging. Radiology 1984;153(1):189–194.

13. Ma J. Dixon techniques for water and fat imaging. J Magn Reson Imaging 2008;28(3):543–558.

14. Bley TA, Wieben O, François CJ, Brittain JH, Reeder SB. Fat and water magnetic resonance imaging. J Magn Reson Imaging 2010;31(1):4–18.

15. Özgen A. The value of the T2-weighted multipoint Dixon sequence in MRI of sacroiliac joints for the diagnosis of active and chronic sacroiliitis. AJR Am J Roentgenol 2017;208(3):603–608.

16. Guerini H, Omoumi P, Guichoux F, et al. Fat suppression with Dixon techniques in musculoskeletal magnetic resonance imaging: a pictorial review. Semin Musculoskelet Radiol 2015;19(4):335–347.

17. Zhadanov SI, Doshi AH, Pawha PS, Corcuera-Solano I, Tanenbaum LN. Contrast-enhanced Dixon fat-water separation imaging of the spine: added value of fat, in-phase and opposed-phase imaging in marrow lesion detection. J Comput Assist Tomogr 2016;40(6):985–990.

18. Douis H, Davies AM, Jeys L, Sian P. Chemical shift MRI can aid in the diagnosis of indeterminate skeletal lesions of the spine. Eur Radiol 2016;26(4):932–940.

19. Low RN, Austin MJ, Ma J. Fast spin-echo triple echo dixon: Initial clinical experience with a novel pulse sequence for simultaneous fat-suppressed and nonfat-suppressed T2-weighted spine magnetic resonance imaging. J Magn Reson Imaging 2011;33(2):390–400.

20. Park HJ, Lee SY, Rho MH, et al. Usefulness of the fast spin-echo three-point Dixon (mDixon) image of the knee joint on 3.0-T MRI: comparison with conventional fast spin-echo T2 weighted image. Br J Radiol 2016;89(1062):20151074.

21. Kirchgesner T, Perlepe V, Michoux N, Larbi A, Vande Berg B. Fat suppression at 2D MR imaging of the hands: Dixon method versus CHESS technique and STIR sequence. Eur J Radiol 2017;89:40–46.

22. Ma J, Singh SK, Kumar AJ, Leeds NE, Zhan J. T2-weighted spine imaging with a fast three-point dixon technique: comparison with chemical shift selective fat suppression. J Magn Reson Imaging 2004;20(6):1025–1029.

23. Ma J, Costelloe CM, Madewell JE, et al. Fast dixon-based multisequence and multiplanar MRI for whole-body detection of cancer metastases. J Magn Reson Imaging 2009;29(5):1154–1162.

24. Pasoglou V, Michoux N, Peeters F, et al. Whole-body 3D T1-weighted MR imaging in patients with prostate cancer: feasibility and evaluation in screening for metastatic disease. Radiology 2015;275(1):155–166.

25. Lecouvet FE, El Mouedden J, Collette L, et al. Can whole-body magnetic resonance imaging with diffusion-weighted imaging replace Tc 99m bone scanning and computed tomography for single-step detection of metastases in patients with high-risk prostate cancer? Eur Urol 2012;62(1):68–75.

26. Lecouvet FE, Geukens D, Stainier A, et al. Magnetic resonance imaging of the axial skeleton for detecting bone metastases in patients with high-risk prostate cancer: diagnostic and cost-effectiveness and comparison with current detection strategies. J Clin Oncol 2007;25(22):3281–3287.

27. Woo S, Kim SY, Kim SH, Cho JY. Journal Club: Identification of bone metastasis with routine prostate MRI: a study of patients with newly diagnosed prostate cancer. AJR Am J Roentgenol 2016;206(6):1156–1163.

28. DeLong ER, DeLong DM, Clarke-Pearson DL. Comparing the areas under two or more correlated receiver operating characteristic curves: a nonparametric approach. Biometrics 1988;44(3):837–845.

29. Landis JR, Koch GG. The measurement of observer agreement for categorical data. Biometrics 1977;33(1):159–174.

30. Schmidt GP, Schoenberg SO, Schmid R, et al. Screening for bone metastases: whole-body MRI using a 32-channel system versus dual-modality PET-CT. Eur Radiol 2007;17(4):939–949.

31. Schmidt GP, Baur-Melnyk A, Haug A, et al. Comprehensive imaging of tumor recurrence in breast cancer patients using whole-body MRI at 1.5 and 3 T compared to FDG-PET-CT. Eur J Radiol 2008;65(1):47–58.

32. Qu X, Huang X, Yan W, Wu L, Dai K. A meta-analysis of ^{18}FDG-PET-CT, ^{18}FDG-PET, MRI and bone scintigraphy for diagnosis of bone metastases in patients with lung cancer. Eur J Radiol 2012;81(5):1007–1015.

33. Simpfendorfer CS, Ilaslan H, Davies AM, James SL, Obuchowski NA, Sundaram M. Does the presence of focal normal marrow fat signal within a tumor on MRI exclude malignancy? An analysis of 184 histologically proven tumors of the pelvic and appendicular skeleton. Skeletal Radiol 2008;37(9):797–804.

34. Vande Berg BC, Lecouvet FE, Michaux L, Ferrant A, Maldague B, Malghem J. Magnetic resonance imaging of the bone marrow in hematological malignancies. Eur Radiol 1998;8(8):1335–1344.

35. Schweitzer ME, Levine C, Mitchell DG, Gannon FH, Gomella LG. Bull's-eyes and halos: useful MR discriminators of osseous metastases. Radiology 1993;188(1):249–252.

36. Erly WK, Oh ES, Outwater EK. The utility of in-phase/opposed-phase imaging in differentiating malignancy from acute benign compression fractures of the spine. AJNR Am J Neuroradiol 2006;27(6):1183–1188.

37. Ragab Y, Emad Y, Gheita T, et al. Differentiation of osteoporotic and neoplastic vertebral fractures by chemical shift in-phase and out-of phase MR imaging. Eur J Radiol 2009;72(1):125–133.

38. Zajick DC Jr, Morrison WB, Schweitzer ME, Parellada JA, Carrino JA. Benign and malignant processes: normal values and differentiation with chemical shift MR imaging in vertebral marrow. Radiology 2005;237(2):590–596.

39. Karanicolas PJ, Bhandari M, Kreder H, et al. Evaluating agreement: conducting a reliability study. J Bone Joint Surg Am 2009;91(Suppl 3):99–106.

40. Raissaki M, Demetriou S, Spanakis K, et al. Multifocal bone and bone marrow lesions in children - MRI findings. Pediatr Radiol 2017;47(3):342–360.

41. Lecouvet FE, Simon M, Tombal B, Jamart J, Vande Berg BC, Simoni P. Whole-body MRI (WB-MRI) versus axial skeleton MRI (AS-MRI) to detect and measure bone metastases in prostate cancer (PCa). Eur Radiol 2010;20(12):2973–2982.

42. Lecouvet FE, Vande Berg BC, Malghem J, Omoumi P, Simoni P. Diffusion-weighted MR imaging: adjunct or alternative to T1-weighted MR imaging for prostate carcinoma bone metastases? Radiology 2009;252(2):624.